Mechanisms of Silk Fibroin Sol−Gel Transitions

Akira Matsumoto,[†] Jingsong Chen,[†,‡] Adam L. Collette,[†,‡] Ung-Jin Kim,[†] Gregory H. Altman,[†,‡] Peggy Cebe,[§] and David L. Kaplan*[,†]

Departments of Biomedical Engineering, Chemical and Biological Engineering, Bioengineering & Biotechnology Center and Departments of Physics and Astronomy, Tufts University, Medford, Massachusetts 02155, and Tissue Regeneration, Inc., Sommerville, Massachusetts 02143

Received: November 3, 2005; In Final Form: July 11, 2006

Silk fibroin sol−gel transitions were studied by monitoring the process under various physicochemical conditions with optical spectroscopy at 550 nm. The secondary structural change of the fibroin from a disordered state in solution to a β-sheet-rich conformation in the gel state was assessed by FTIR and CD over a range of fibroin concentrations, temperatures, and pH values. The structural changes were correlated to the degree of gelation based on changes in optical density at 550 nm. No detectable changes in the protein secondary structure (FTIR, CD) were found up to about 15% gelation (at 550 nm), indicating that these early stages of gelation are not accompanied by the formation of β-sheets. Above 15%, the fraction of β-sheet linearly increased with the degree of gelation. A pH dependency of gelation time was found with correlation to the predominant acidic side chains in the silk. Electrostatic interactions were related to the rate of gelation above neutral pH. The overall independencies of processing parameters including concentration, temperature, and pH on gel formation and protein structure can be related to primary sequence-specific features in the molecular organization of the fibroin protein. These findings clarify aspects of the self-assembly of this unique family of proteins as a route to gain control of material properties, as well as for new insight into the design of synthetic silk-biomimetic polymers with predictable solution and assembly properties.

Introduction

Silks are fibrous proteins spun by some lepidoptera larvae such as silkworms, and other arthropods including spiders, scorpions, mites, moths, butterflies, wasps, and bees.[1,2] Silkworm silk from *Bombyx mori*, the most extensively characterized silk, has been used in textile production for centuries and more recently as biomedical sutures. There are two main protein components in the *Bombyx mori* silkworm silk. The predominant component is fibroin, a hydrophobic structural protein consisting of heavy and light chains present in equimolar rations with molecular masses of ca. 390 and ca. 25 kDa, respectively, bonded together by a single disulfide bond.[3,4] The other component, sericin, constitutes 25−30% of the silk proteins in cocoons and is part of a family of hydrophilic "glue-like" proteins that holds the hydrophobic fibroin monofilaments together forming a silk fiber.[5]

The primary structure of fibroin consists of a predominance (ca. 90%) of the amino acids (glycine, alanine, serine, valine, and tyrosine) with characteristic repetitive sequences of GAGAGS, GAGAGY, and GAGAGVGY,[6] which are responsible for the formation of antiparallel β-sheets in the spun fibers. This β-sheet formation ultimately contributes to the stability and the remarkable mechanical features of spun silk fibers.[7] Fibroins are composed of relatively large hydrophilic chain end blocks (N- and C-termini) with smaller hydrophilic internal blocks and large internal hydrophobic blocks where the repeats listed above are encoded.[8,20,21]

The silk glands of *B. mori* consist of three divisions: the posterior, middle and anterior divisions, and the spinning duct. The silk fibroin is synthesized and forms a gel in the posterior division, is stored in the middle division, and is then transported to the anterior division prior to being spun into fiber in the spinning duct.[9] Along the processing path, changes in the physiological conditions such as pH, concentration of salts (monovalent and divalent), and content of water occur. Although the entire process has not been fully recapitulated in vitro, these changes control solubility, polymer assembly, and structural organization of this unique protein before it is spun into a solid fiber.[10]

The biocompatibility of the fibroin protein has been extensively addressed,[11−14] and unlike collagen, another naturally derived fibrous protein, there is no bioburden associated with silks.[11] Due to the β-sheet formation, silks exhibit relatively slow degradation in vitro and in vivo when compared to collagens and many other biopolymers.[11,15] This feature makes the use of silk, specifically in biomaterial formats for tissue engineering, advantageous when compared with most other natural or synthetic polymers, allowing for maintenance of the mechanical integrity during new tissue formation.[16,17] The combination of excellent mechanical properties, options for genetic control of sequence to tailor structure and function, and biocompatibility provides a solid platform for a wide range of biomaterial options with silk. Importantly, silk fibroin is versatile in terms of processability and has been successfully formed into many different material formats by using biologically relevant conditions of water, ambient temperature, and physiologically relevant chemicals where needed. Silk-based biomaterial designs include films,[18−20] nanoscale diameter fibers via electrospinning,[21,22] fiber textile bundles,[23,24] 3D porous scaffolds,[16,17] and hydrogels.[25]

[†] Departments of Biomedical Engineering, Chemical and Biological Engineering, Bioengineering & Biotechnology Center, Tufts University.
[‡] Tissue Regeneration, Inc.
[§] Departments of Physics and Astronomy, Tufts University.

10.1021/jp056350v CCC: $33.50
Published on Web 10/04/2006

Silk gels form with treatments such as shearing (spinning), water evaporation (or water exclusion from the bulk via osmotic stress), solvent exposure, or heating. Gels are stabilized due to the formation of thermodynamically stable β-sheets, which serve as physical cross-links to stabilize gels and are essentially irreversible under physiological conditions unless degraded due to enzymatic or oxidative processes. A number of other biodegradable hydrogel systems based on naturally derived and biocompatible polymers have been studied and found biological applicability.[26] Typically, these systems involve polysaccharides and their derivatives, or proteins that form thermally induced physical networks. Compared to these systems, the rate of silk gelation, in general, is unusually slow. As described earlier, hydrophobic domain mapping of the fibroin sequence illustrates the amphiphilic (hydrophobic and hydrophilic segments) nature of the protein.[10,27] On the basis of this block copolymer evolutionary design, a soft-micelle assembly process was demonstrated for these proteins, as well as a critical role for the shorter hydrophilic blocks (intervening between larger hydrophobic and crystalline blocks) to prevent premature β-sheet formation and to modulate water solubility.[27] Understanding factors governing silk gelation and the mechanisms involved is important for improved handling of this unique protein as well as for guidance for other (natural or synthetic) polymer designs in terms of optimizing processing and functionalization of materials formed from these polymers, particularly when assembled in an aqueous environment.

In the present study, we investigate silk fibroin sol−gel transition processes in detail. A focus was placed on quantitative changes in gel formation concurrent with secondary structure to develop a mechanistic picture of the processes involved. The effects of physical parameters such as fibroin concentration, temperature, and pH on gelation and structure were determined and suggest a two-step model for the sol−gel transition.

Materials and Methods

Preparation of the Silk Fibroin Aqueous Solutions. Degummed (sericin free) *B. mori* silk was prepared by our previously established methods[20] with the following modifications. Bave silk (Rudolph-Desco Co. Inc., NJ) was used as a starting material instead of cocoon. The bave silk was boiled for 1 h in an aqueous solution of 0.02 M Na_2CO_3 in the presence of 0.3% bleach to extract the glue-like sericin proteins. The extracted silk (fibroin) was then thoroughly rinsed 7 times with heated (65 °C) and cold water. The fibroin was dissolved in 9.3 M LiBr solution at 60 °C for 4 h, yielding a 20 w/v % solution. This solution was dialyzed against distilled water, using Slide-a-Lyzer dialysis cassettes (MWCO 3500, Pierce), for 2 days with 6 changes of water. All the water used was Milli-Q (Millipore Corp.). The terminal concentration of the fibroin solution after dialysis was 7.2 w/v %, determined by weighing the remaining solid after drying. Amino acid analysis was conducted to assess protein purity and no sericin protein contamination was found. Removal of Li^+ ion was verified by XPS X-ray photoelectron spectrometer (ESCA SSX-100, Surface Science), in which no Li^+ ion peak was observed. A series of concentrations of the fibroin solution were prepared by diluting the 7.2 w/v % solution with distilled water. Samples with different pH values were prepared by adding 0.1 and 0.01 M of HCl and NaOH, respectively, followed by addition of water conditioned to a series of NaCl concentrations to adjust the final concentrations of fibroin and salt. NaCl was added to the solutions to obtain weight ratios to fibroin that reflect that of the lowest reported in the silk gland in vivo during the fibroin processing into fibers (15 μg/g).[28] All the diluted, pH, and salt conditioned solutions were stored overnight at 4 °C to achieve homogeneity and to avoid any premature precipitation of the protein, which can occur at room temperature. The pH of the solutions was determined prior to gelation experiments.

Monitoring Gelation. Gelation was conducted in covered 96-well plates (MICROTEST 96, Falcon, USA) and incubated in a light-free environment either at room temperature or at 37 °C. A 200 μL volume of fibroin solution was gently pipetted onto each well to avoid shear effects. To follow the gelation process and to determine gelation time, turbidity changes at 550 nm were monitored with a Microplate Reader System VERSAmax (Molecular Devices, CA). Fibroin gelation yields a heterogeneous microstructure and thus causes an increased degree of light scattering in the visible light range, leading to an increase in the turbidity. This change is defined as optical density (OD) change, which was measured and presented in the absorbance mode (550 nm). For each concentration of fibroin, 12 wells were used and the values were averaged to obtain the time-course optical density changes. Gelation time was defined as the time point where the average optical density reached half-maximum value. For all cases, the degree of gelation (*d)* was defined as follows: $d = (OD - OD_{min})/(OD_{max} - OD_{min})$, where OD is the optical density measured at a certain point of time, and OD_{min} and OD_{max} are the smallest and largest optical densities measured, respectively. For conducting experiments correlating gelation degree (*d*) to evolving structural changes (Figures 6−8), many pre-gel solution samples were first prepared and then incubated (at either room temperature or 37 °C) at different time frames to improve tracking of partially gelled samples.

Fourier Transform Infrared Spectroscopy (FTIR). FTIR analysis was conducted with a Bruker EQUINOX 55 FTIR spectrophotometer (Bruker, USA). For each spectrum, a 128-scan interferogram was collected at single beam absorption mode with a 2 cm^{-1} resolution and a 1 cm^{-1} interval from the 4000 to 400 cm^{-1} region. All spectral manipulations were performed with OPUS (version 4.2) software (MATTSON INSTRUMENT, INC.). Quantification of secondary structure was based on analyzing the amide I region (1600−1700 cm^{-1}).[29,30] Background absorption due to water was subtracted from the sample spectra to obtain a flat recording in the range of 1750−2000 cm^{-1}.[31] Second derivative spectra were obtained from the sample spectrum by using a third degree polynomial function with a 9-point Savitski−Golay smoothing function.[31] A linear baseline was used and for initial deconvolution only the frequencies detected by second derivative analysis were used as peak maxima.[31,32] Throughout the process deconvoluted peak shapes were assumed to be mixed Gaussian and Lorentzian and were allowed to vary within a 0−100% mixture ratio.[32] The average percent composition of fibroin secondary structure for the series of samples,[33,34] specifically the amount of β-sheet structure, was assessed by integrating the area of each deconvoluted curve and then normalizing to the total area of the amide I region.

Circular Dichroism. Circular dichroism (CD) spectra were recorded with a 0.01 mm path length, sandwich cell (Hellma QS-666) at concentrations of 0.45 and 0.9 w/v % on a Jasco-720 CD spectrophotometer (Jasco Co., Japan). All samples were scanned at 25 °C with a 4-s accumulation time at the rate of 100 nm/min, and the results were averaged from at least three repeated experiments. Two major time-dependent points were identified in the spectra at 199 and 217 nm, attributable to changes in fraction of random coil and β-sheet conformations,

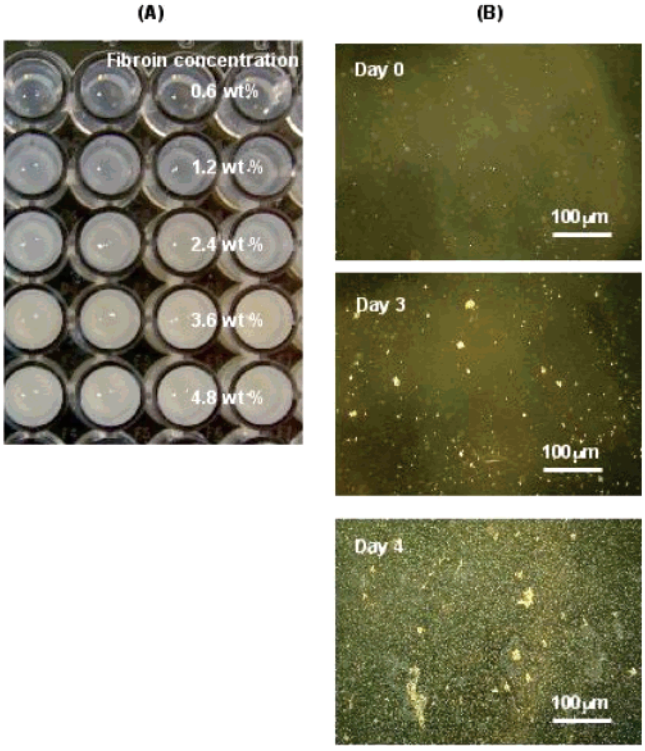

Figure 1. Light microscope images of (A) fibroin gels at various concentrations prepared at 37 °C with 200 μL in 96-well plates and of (B) fibroin solutions of 400 μL in a 12 well plate for 3.6 wt % at different incubation times to show sol−gel transitions.

respectively.[35−37] The CD fraction changes (f) at these wavelengths were calculated as follows: $f = (\theta - \theta_{min})/(\theta_{max} - \theta_{min})$, where θ is the ellipticity at each wavelength (199 and 217 nm), and θ_{min} and θ_{max} are the smallest and largest ellipticities measured, respectively. These fraction changes (f) were monitored and plotted as a function of degree of gelation (d) to represent conformational changes during the sol−gel transition.

Results

Influence of Concentration and Temperature on Fibroin Gelation. Upon gelation, fibroin yielded an opaque white color (Figure 1A) due to the heterogeneous microstructure of the fibroin gel causing light scattering in the visible light range. Accordingly, to track gelation optical density changes at 550 nm were monitored. This approach permitted screening of small volumes in microliter plate formats, with 200 μL per well. During early stages of gelation small precipitates (<10 μm) first appear and the sizes of these precipitates gradually increase leading to increases in optical density (Figure 1B). In later stages of the gelation process, larger aggregates (10−100 μm) become immobile in the bulk or partially gelled state. This state lasts several hours and finally overall gelation takes place. Optical density changes with time for fibroin solutions of various concentrations at (a) room temperature and (b) 37 °C (Figure 2). The optical densities stabilize at the values where all solutions (12 samples evaluated for each condition) have gelled, with final values correlating with the initial concentration of fibroin. The slightly different final level of optical density (in the gel state) between the two temperatures was due to occasional deformation or cracking of gels. The observed optical density changes were associated with changes in β-sheet structure in the fibroin gels, as described in the next section. Changes in optical density were identified as an indicator of change in fibroin secondary structure during the gelation transition. Relationships between gelation time and the fibroin concentration at room temperature and 37 °C are shown in Figure 3. Gelation time decreased with an increase in fibroin concentration and temperature, although the concentration dependency becomes less evident below 1 wt %. This trend is consistent with our previous work where the fibroin gelation time was qualitatively defined as the time point when the fibroin solution did not flow from an inverted vial.[17]

Secondary Structure of Fibroin during Gelation. FTIR analysis was carried out to assess secondary structural changes of the fibroin during the sol−gel transition for various concentrations and temperatures. Figure 4 shows spectral changes of fibroin concentration of 7.2 wt % determined at room temperature for sol (A) and gel states (B). As can be seen in Figure 4, the peaks of the overlapped (before deconvolution) amide I bands (1600−1700 cm^{-1}) shift from 1650 to 1625 cm^{-1} after gelation. A shift of the amide II (1500−1600 cm^{-1}) peak from 1550 to 1535 cm^{-1} was also observed. These transitions reflect the increased fraction of the peak components in the ranges of 1620−1625 (amide I),[29−31,34] 1697−1703 (amide I),[30,38] and around 1516 cm^{-1} (amide II),[39] all attributable to the β-sheet structure, and the correspondingly decreased fraction of disor-

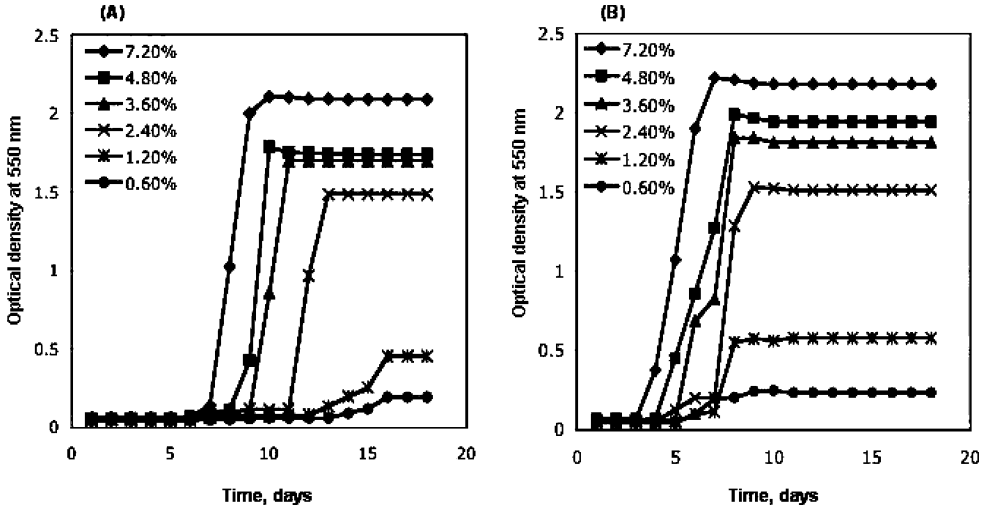

Figure 2. Optical density changes (at 550 nm) of the fibroin solutions at 200 L in a 96 well plate for various fibroin concentrations prepared at (A) room temperature and (B) 37 °C. Twelve samples were taken for each condition and averages are displayed. Standard deviations ranged from 0.02 to 0.31 and 0.01 to 0.26 in panels A and B, respectively.

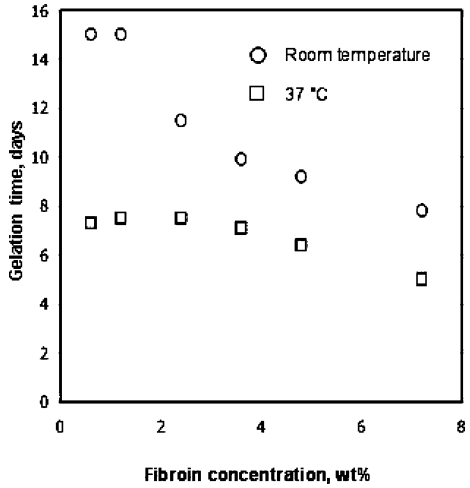

Figure 3. Concentration-dependent fibroin gelation time at (○) room temperature and (□) 37 °C determined from optical density changes at 550 nm.

dered silk structures that give rise to bands in the range of 1640−1660 cm^{-1} (amide I)[29−31,34,38] and around 1535 [1] cm^{-1} (amide II).[39,40] The fraction change of the β-sheet structure over time during gelation were assessed by deconvolution peak analysis for the various fibroin concentrations at 37 °C and room temperature (Figure 5). Initially (sol state), all the solutions regardless of concentration had approximately 20% content of β-sheet. This value remained constant until the degree of gelation reached 15−20% (Figure 6) and then increased. Once the gelation was completed there was no significant change in the fraction of the β-sheet structure. For the lowest fibroin solution concentration of 0.9 wt % the extent of β-sheet formation in the terminal gel state reached around 50%. Also, despite the higher rate of gelation at 37 °C than at room temperature, there was no difference in terms of the fractional changes in β-sheet structure. The change in β-sheet fraction at room temperature was plotted against the degree of gelation as determined from optical density changes for the various fibroin concentrations in Figure 6. It can be seen that the fraction of β-sheet does not increase until reaching a 15−20% degree of gelation. The delayed increase in β-sheet increase indicates that initial stages of silk fibroin gelation are not accompanied by the formation of β-sheet structures discernible via FTIR. These early stage interactions likely represent inter- or intramolecular hydrophobic interactions to form physical cross-links that subsequently mature into β-sheet structures as sheet stacking ensues. It is possible that some hydrogen bonding and electrostatic interactions are also responsible for the gelation process

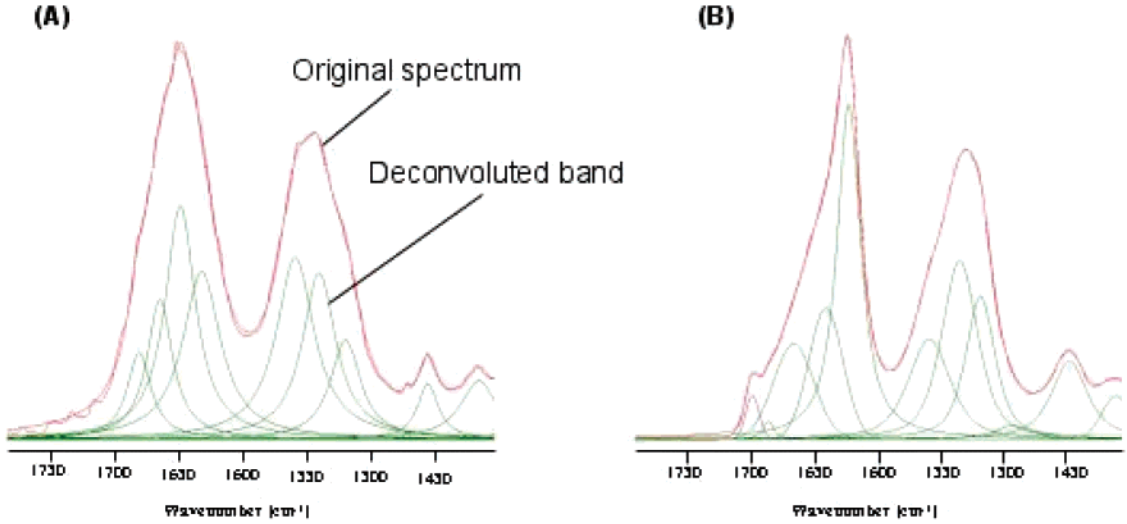

Figure 4. Representative FTIR spectra of fibroin (A) solution and (B) gel at room temperature for 7.2 wt % shown with deconvoluted peaks.

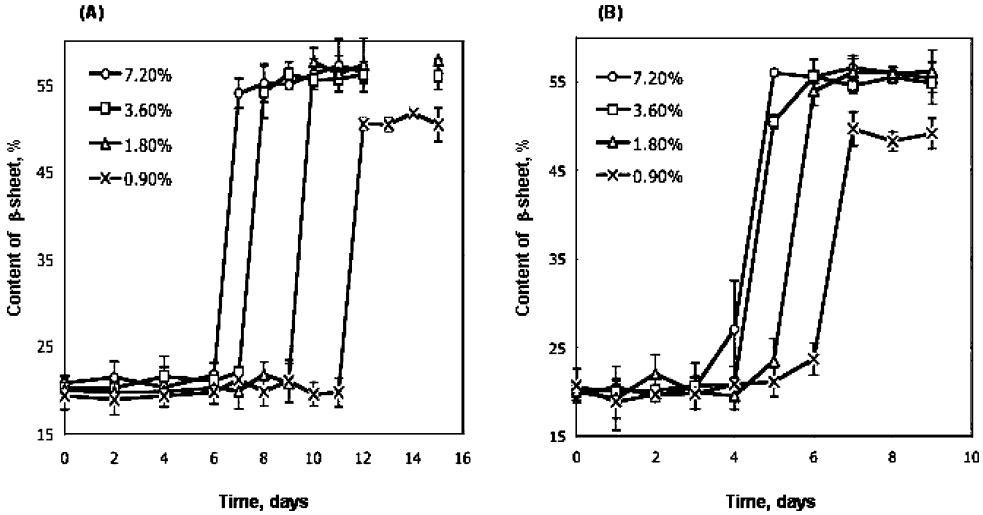

Figure 5. Changes in β-sheet fraction during the sol−gel transitions as a function of time assessed by FTIR amide I band (1600−1700 cm^{-1}) analysis for various fibroin concentrations at (A) room temperature and (B) 37 °C: 7.2 (○), 3.6 (□), 1.8 (△), and 0.9 wt % (×).

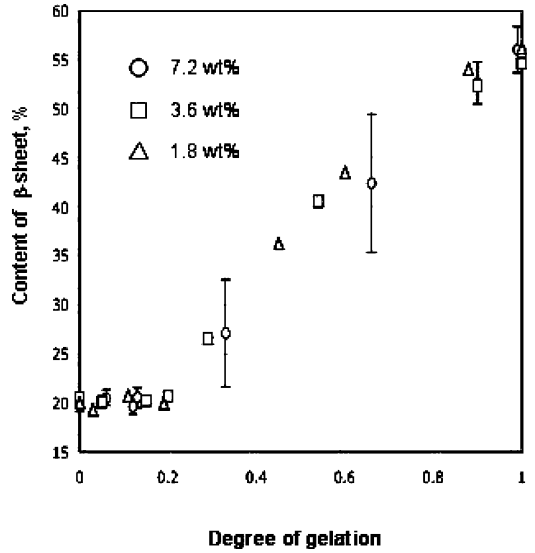

Figure 6. Fraction of β-sheet during gelation as a function of extent of gelatin, determined by optical density at room temperature for 7.2 (○), 3.6 (□), and 1.8 wt % (△).

at these early stages, but are likely less contributory to the transition than the dominating hydrophobic interactions. This issue is further discussed below.

To further refine our understanding of the conformational changes of the fibroin chains during these transitions, CD spectra were monitored during gelation. Figure 7 shows the time-course of spectral changes for concentrations of (a) 0.9 and (b) 0.45 wt %. Initially, the spectra show characteristic features of random coil with a weak shoulder at 217 nm and a relatively strong band at 199 nm. However, as gelation proceeds the negative band at 217 nm becomes stronger, yielding a minimum point, and simultaneously the band at 199 nm declines and becomes a positive maximum point in the final gel spectra, characteristic of β-sheet structures. Figure 8 shows normalized band intensity changes at both wavelengths: 199 and 217 nm, as a function of the degree of gelation. As gelation proceeds, the intensity at 199 nm increases, whereas the intensity at 217 nm decreases, corresponding to decreased random coil content and increased β-sheet content, respectively. Similar to the observations in Figure 6, a slightly delayed commencement of the CD changes to the change of optical density (degree of gelation) is observed (Figure 8).

Effect of pH on Fibroin Gelation Time and Secondary Structure. Figure 9 shows relationships between gelation time and initial solution pH for fibroin concentrations of 1.8 and 3.6 wt % based on optical density changes at room temperature. Strong pH-dependent changes in gelation time were observed. For both concentrations, gelation time increased with increased pH with significant increases notable in the range of pH 4−6 and 9−10.5, with a less dramatic change in the range of pH 6−9. When comparing both concentrations at the same pH, a shorter gelation time was obtained for the higher fibroin concentration (3.6 wt %). The gel curves (Figure 9) represent titration-like curves of the fibroin with acidic and basic group pK_a values at around 4.5 and 10, respectively, corresponding to the points along the curves where gelation times change most sensitively to changes in the pH. Over the range of pH it appears that protonation of the side chain carboxyl group plays a dominant role in determining gelation rate. From neutral to acidic pH, neutralizing carboxyl groups proceeds, resulting in reduced hydrophilicity and reduced charge repulsion. This should promote hydrophobic interactions of fibroin molecules and thus more physical cross-links and quicker gelation. Although basic groups exist in the fully charged state in this range of pH and are thus available for electrostatic interactions with carboxyl groups, hydrophobic interactions dominate the process due to the content when compared to the relatively small hydrophilic domains. In the neutral range (pH 6−9) where both acidic and basic groups are mostly charged, electrostatic interactions between the oppositely charged groups should predominate, also providing opportunities for fibroin chain interactions. This may be the reason for the relatively shorter gelation times in the neutral pH range when compared to those for more basic conditions. When the pH increased above 9, deprotonation of the basic groups begins whereas the acidic groups are fully deprotonated (charged), and thus the effect of electrostatic interaction decreases or could become repulsive, leading to an increase in gelation time. Figure 10 shows the fractions of β-sheet structures in the sol and gel states at the various pH values and concentrations determined from FTIR amide I band analysis. There is no significant pH dependency except for a few points in the very acidic (lower than pH 4)

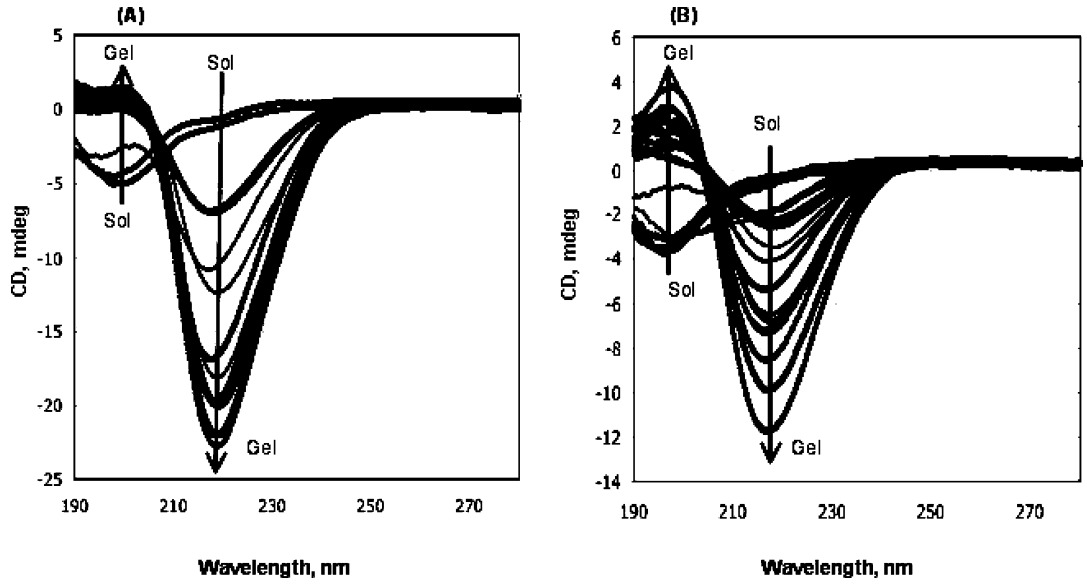

Figure 7. CD spectra of fibroin during gelation at room temperature for (A) 0.9 and (B) 0.45 wt %.

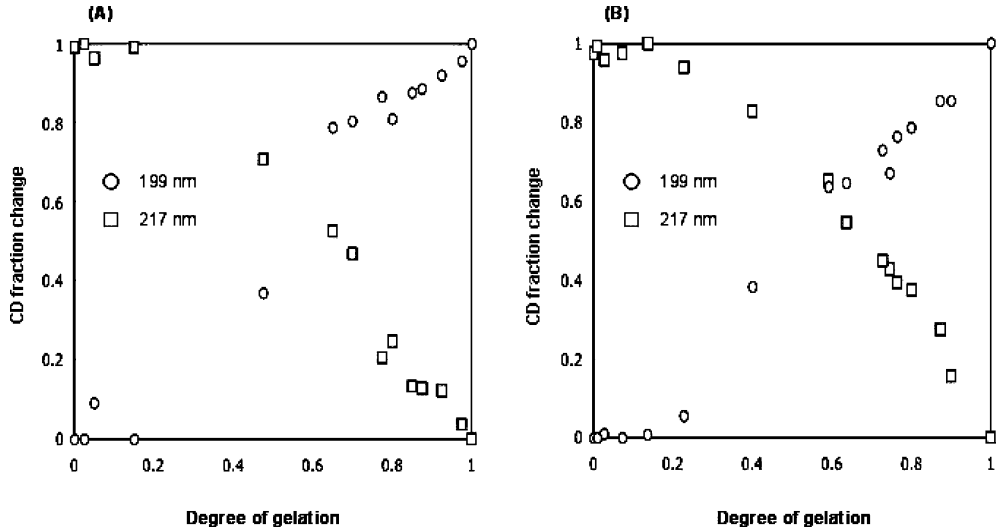

Figure 8. CD spectral changes during gelation as a function of degree of gelatin, determined by optical density at room temperature for (A) 0.9 and (B) 0.45 wt %.

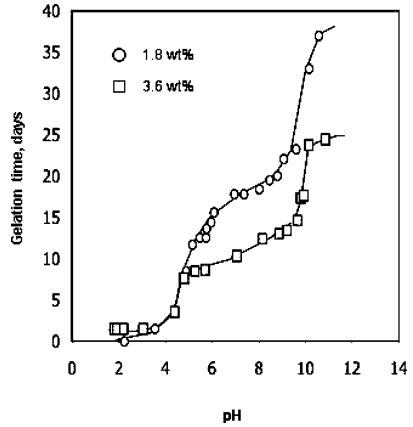

Figure 9. Relationships between initial solution pH and gelation time at room temperature determined by change in the optical density for (○) 1.8 and (□) 3.6 wt %.

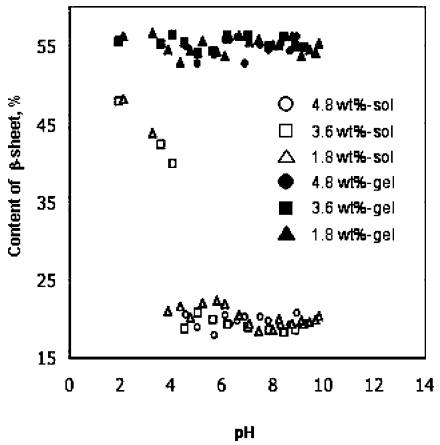

Figure 10. pH effects on β-sheet fraction at room temperature assessed by FTIR amide I band (1600−1700 cm^{-1}) analysis for various fibroin concentrations.

range, showing intermediate values between sol and gel states. This effect occurred because these highly acidic solutions began geling as soon as they were prepared. The 4.8% solution gelled immediately after adjusting the pH below 4, and thus plots in this range are not included. When these acidic solutions gelled, the content of the β-sheet was in the same range as other samples, suggesting that the fraction of β-sheet in the fibroin gel is independent of processing pH.

Discussion

The sol−gel transition of fibroin arises from a combination of inter- and intramolecular interactions including hydrophobic interactions and hydrogen bonds leading to β-sheet formation, resulting in physical cross-links.[25,41,42,43] Increased fibroin concentration provides the increased chain interactions and thus accelerates gelation (Figure 3).

The accelerated gelation at higher temperature can be explained by the dynamics of hydrophobic hydration.[44] For a number of synthetic polymers as well as polypeptides with modulated balance of apolar (hydrophobic) and polar (hydrophilic) moieties, such as those found in elastin-like peptides [poly(VAPGVG)$_n$][45] and silk-elastin-like polymers (SELPs),[46] temperature-induced reversible phase separation has been recognized, where the polymers are soluble in water at low temperature but precipitate upon increasing the temperature. In the soluble state, the hydrophobic moieties within the polymers are surrounded by ice-like (ordered) water (water of hydrophobic hydration).[47] Increasing temperature leads to phase separation (or protein folding).[48] In the case of most synthetic polymers or the elastin systems mentioned above,[44,45] this process is reversible; upon cooling the precipitate redissolves in water. However, in the case of the silk fibroin protein this localized dehydration process results in irreversible β-sheet formation due to the thermodynamic stability of this secondary structure. As shown in Figures 6 and 8 where the β-sheet fraction and optical density changes were monitored in parallel, the early stage of gelation was not accompanied with β-sheet formation, suggesting that this early stage of fibroin gelation is reversible (Figure 11). Indeed, such reversible fibroin gelation has been previously reported, where the solution pH was shifted by applying acidic or basic vapors.[49] The cycle could be repeated provided that the fibroin remained in a gel state only for a few minutes. This observation supports the concept that the early stage of fibroin gelation is induced by relatively weak interactions (e.g., limited hydrogen bonding or limited domains of hydrophobic interactions) that do not involve β-sheet formation (Figure 11).

The β-sheet content (average percentage composition of all other secondary structures detected as amide I bands) in the solution state was unexpectedly high (20%). However, this value

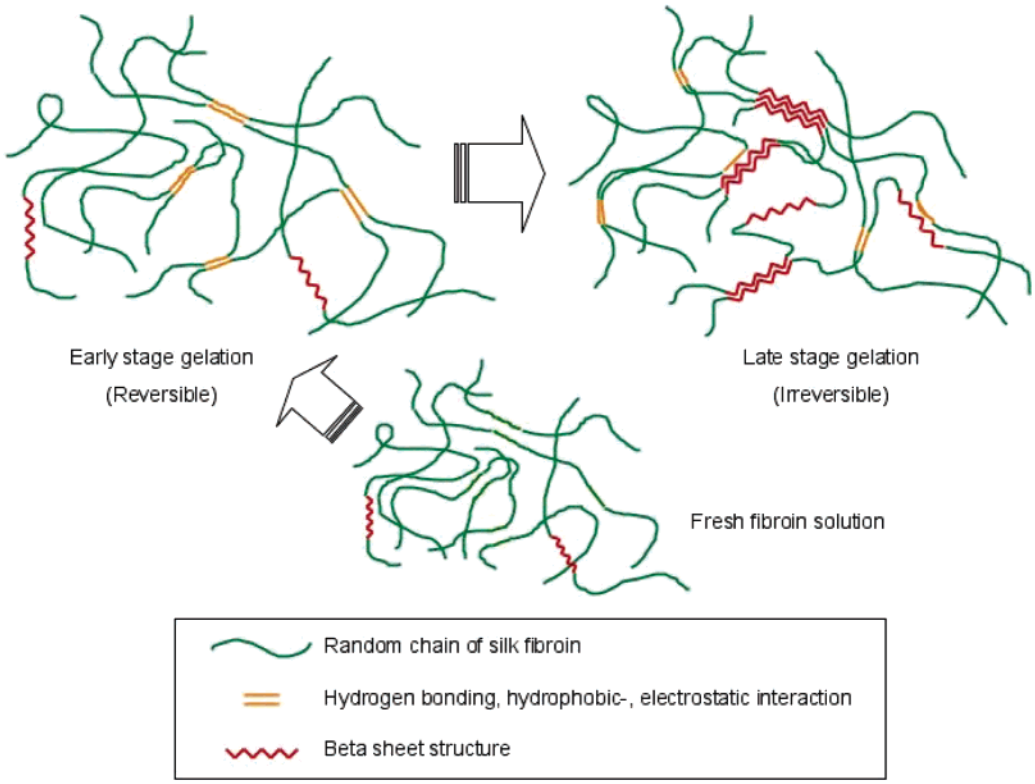

Figure 11. Schematic illustration of pregelation and early and late stages of fibroin gelation, a three-stage model. A fresh solution (pregelation) has about 20% content of β-sheet structures with negligible intermolecular bindings (A); gelation is initially induced by weaker interchain interactions such as (non-β-sheet forming) hydrogen bonding, hydrophobic interactions, and electrostatic interactions (B); and stable β-sheet structures cure in the third phase resulting in stable and essentially irreversible intermolecular structures (C).

corresponds to data on the secondary structure found in films cast with concentrations of fibroin of 2.5−2.8 w/v % and assessed with similar FTIR amide I band analysis.[34] It has been shown that the fraction of β-sheet increases significantly with increase in casting temperature and was as high as 15% when the film was cast at room temperature.[34] It has also been shown by ^{13}C CP-MAS NMR spectral deconvolution that the content of total silk II (β-sheet-rich) conformation of fibroin cast film was 22% at a pH in the range of 6.9−8.0.[50] Recently, the compositions of β-sheet structure in concentrated [26% (w/w)] fibroin solutions have also been quantified based on Raman spectroscopy and the deconvoluted amide I band analysis for regenerated as well as native solutions (extracted from middle division of *B. mori* silk gland) and were reported to contain 25% β-sheet structure.[51] The relatively high β-sheet content observed in the present study and these other reports may be attributable to the higher fibroin concentration during solution preparation. In the present study 20 w/v % in LiBr solution was used, yielding a 7.2 w/v % solution after 2 days of dialysis. The higher concentration together with 2 days of incubation at room temperature (during dialysis) could promote intra- and intermolecular interactions of the fibroin chains leading to β-sheets. The generality of the observed high content of β-sheet in this solution state may also imply the existence of metastable fibroin structures within this range of β-sheet fraction, likely formed from intramolecular interactions.

The pH dependency of gelation shown in Figure 10 illustrates the important role of carboxyl groups (Glu and Asp) in determining fibroin chain interactions. The heavy chain N-terminus of the fibroin of *B. mori*, the large hydrophilic domain, is dominated by negatively (acidic) charged amino acid side chains with a ratio of 5:3 to positively charged groups (the predicted p*I* is 4.59), whereas the C-terminus, the other relatively large hydrophilic domain, has a predominance of positive charges with a ratio of 9:1 (the predicted p*I* is 10.53). The light chain that is covalently linked by a disulfide bond to the heavy chain at the C-terminus shows a predominance of acidic groups with a calculated p*I* of 5.06. Note that these p*I* values (4.59, 5.06, and 10.53) closely agree with the observed apparent pK_a values in Figure 10 (ca. 4.5 and 10), where the gelation times were observed to be most sensitive to changes of pH. The predominant role of carboxyl groups in determining the gelation rate may also be attributable to different levels of contribution between carboxyl and amino groups to the overall hydrophilicity/hydrophobicity of the polymer networks.

On the basis of observations of change in lower critical solution temperature (LCST) of amphiphilic copolymers such as poly(*N*-isopropylacrylamide), it is suggested that amino groups promote hydrophilicity, whereas carboxyl groups promote hydrophobicity, when these groups are present mostly (or completely) in uncharged states.[52−54] This discrepancy between the two groups has been explained by hydrogen bonding formed between uncharged carboxyl groups and amide groups (CONH) such as in poly(*N*-isopropylacrylamide).[54] Unusually strong hydrogen bonding between ionized and neutral carboxyl groups has also been reported.[55,56] The rate of formation of these hydrogen bonds accelerates with a decrease of local dielectric constant, which can be caused by local dehydration[57,58] or interaction with hydrophobic substances.[59,60] Fibroin is essentially a very hydrophobic molecule, where in the soluble (sol) state the majority of the hydrophobic moieties within the molecule must be surrounded by ordered water (water of hydrophobic hydration). In this situation, the entropy of hydration, ΔS (hydration), is negative due to the ordered structure of the water, therefore, increasing temperature leads to a positive contribution ($-T\Delta S$ is positive) to the free energy of hydration

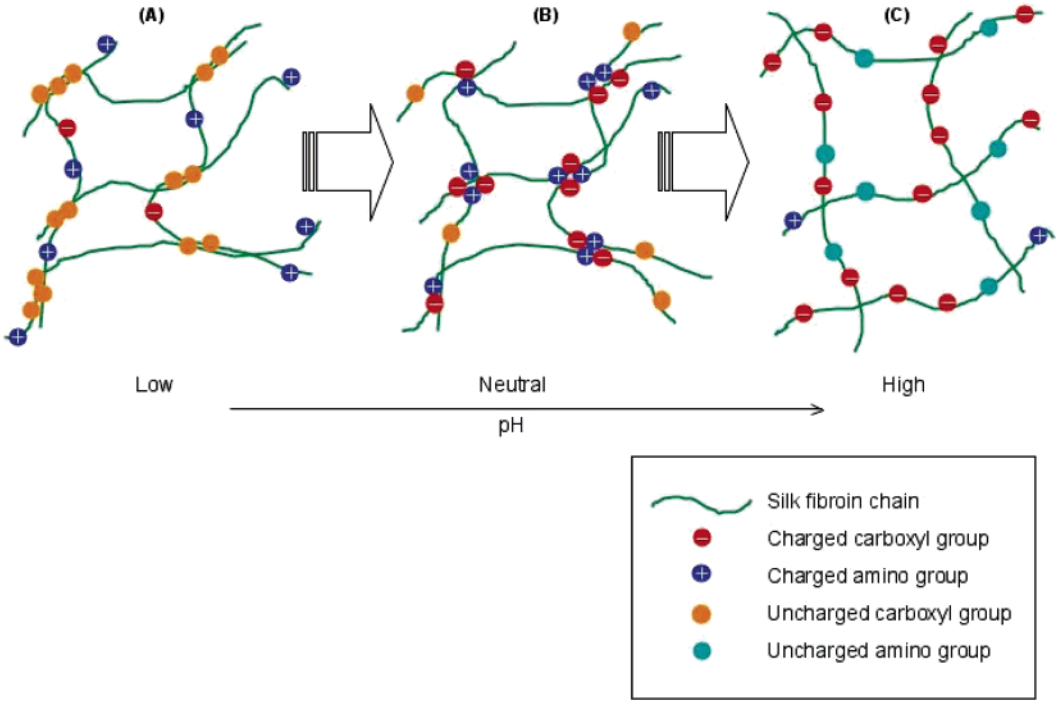

Figure 12. Schematic illustration of pH-dependent fibroin interchain interactions at the early stage of gelation. For simplification, the number ratio of (positive and negative) charges does not represent the actual sequence. At low pH (A), strong interchain aggregation is induced due to increasing hydrophobicity of the uncharged carboxyl group (rapid gelation). At neutral pH (B), there is an increasing effect of electrostatic interactions due to increased number of counterions (relatively rapid gelation). At high pH (C), the interaction is weaker due to increased hydrophilicity of the charged carboxyl group as well as reduced electrostatic interactions (slow gelation).

[solubility in water is limited by Gibbs free energy of solvation given by the following expression: ΔG(hydration) = ΔH(hydration) − $T\Delta S$(hydration)]. When this positive entropic term overwhelms that of heat or enthalpy (ΔH), local dehydration takes place causing a local decrease in dielectric constant.[61] Accordingly, the increased temperature may enhance the hydrogen bonding. Indeed, at 4 °C, a much lower temperature than Figure 10, the pH dependency of the gelation time is different (data not shown); gelation rates at acidic and basic pH are much longer while at neutral pH the rate becomes the fastest. These results suggest that at this lower (4 °C) temperature, electrostatic interactions are more rate determining due to the decreased hydrophobic interactions. Therefore, thermosensitive hydrogen bonding effects are observed.

The pH in the silk gland decreases form 6.9 to 4.8 along the secretory pathway from the posterior to interior divisions.[9] Considering the predicted p*I* values for the N-terminus (4.59) and for the light chain (5.06), this range of pH change (from 6.9 to 4.8) should significantly increase the degree of protonation of carboxyl groups, and thus promote their intra- or intermolecular interactions. Also, from the comparison between these predicted p*I* values (or the apparent pK_a values observed in Figure 9) and the range of pH change occurring in vivo (from 6.9 to 4.8), it can be concluded that the carboxyl groups become charged during in vivo processing and are therefore available for electrostatic interactions with basic groups which are present in the charged (protonated) state under these pH conditions. Thus, the observed faster gelation near neutral pH compared to the basic range (Figure 10) may be attributable to electrostatic interactions more than hydrophobic interactions. These views of the pH-dependent gelation (early stage interchain interactions) process are illustrated in Figure 12. This contribution of electrostatic interactions could be further clarified by investigating the effects of cations such as Na^+, K^+, and Ca^{2+} on the pH−gelation time profile that should affect the fibroin molecular organization by screening electrostatic interactions.

Conclusion

In the present study, the sol−gel transition of silk fibroin was studied with a focus on correlating changes in secondary structure with changes in gelation according to various processing variables: concentration of fibroin, pH, and temperature. Optical density changes at 550 nm were monitored in parallel with the analysis of gel secondary structure, and used to measure the extent of gelation with time. Gelation is initially induced by weaker interactions that do not involve significant secondary structural changes. These initial changes are followed by strong, virtually irreversible β-sheet formation. The study of the pH dependency of fibroin gelation times resulted in the identification of a dominant role for acidic groups in controlling gelation rate, a feature that nicely parallels the process in vivo. In addition, from the observation of the pH−gelation time profiles in the neutral to basic pH range, the contribution of electrostatic interactions to gelation kinetics was suggested. The overall independencies of processing parameters including concentration, temperature, and pH on gel structure suggests sequence-specific control of the molecular organization of fibroin—related both to the hydrophobic regions as well as the chain end hydrophilic sequence blocks. This level of control of sol−gel transitions, when combined with the impressive mechanical properties, biocompatibility, and biodegradability, as well as versatile materials morphological options, suggest increasing options for the use of silks in biomaterial designs and applications.

Acknowledgment. We thank the NIH (P41 EB002520), the NSF (DMR), and TRI, Inc. for support of various aspects of this work.

References and Notes

(1) Kaplan, D. L.; Mello, C. M.; Arcidiacono, S.; Fossey, S.; Senecal, K.; Muller, W. *Protein-Based Materials*; Birkhauser: Boston, MA, 1998; pp 103−131.

(2) Kaplan, D. L.; Adams, W. W.; Farmer, B.; Viney, C. Silk: biology, structure, properties and genetics. In *Silk polymers*: *materials science and biotechnology*; Kaplan, D. L., Adams, W. W., Farmer, B., Viney, C., Eds.; ACS Symp. Ser., No. 544; American Chemical Society: Washington, DC, 1994; p 2.

(3) Tanaka, K.; Kajiyama, N.; Ishikura, K.; Waga, S.; Kikuchi, A.; Ohtomo, K.; Takagi, T.; Mizuno, S. *Biochim. Biophys. Acta* **1999**, *1432*, 92−103.

(4) Zhou, C. Z.; Confalonieri, F.; Medina, N.; Zivanovic, Y.; Esnault, C.; Yang, T.; Jacquet, M.; Janin, J.; Duguet, M.; Perasso, R.; Li, Z. G. *Nucleic Acids Res.* **2000**, *28*, 2413−2419.

(5) Magoshi, J.; Magoshi, Y.; Becker, M. A.; Nakamura, S. In *Polymeric Materials Encyclopedia*; Salamone, J. C., Ed.; CRC Press: New York, 1996; Vol. 1, p 667.

(6) Asakura, T.; Kaplan, D. L. In *Encyclopedia of agricultural science*; Arutzen, C. J., Ed.; Academic Press: New York, 1994; Vol. 4, pp 1−11.

(7) Cunniff, P. M.; Fossey, S. A.; Auerbach, M. A.; Song, J. W.; Kaplan, D. L.; Adams, W. W.; Eby, R. K.; Mahoney, D.; Vezie, D. L. *Polym. Adv. Technol.* **1994**, *5*, 401−410.

(8) Zhou, C. Z.; Confalonieri, F.; Medina, N.; Zivanovic, Y.; Esnault, C.; Yang, T.; Jacquet, M.; Janin, J.; Duguet, M.; Perasso, R.; Li, Z. G. *Nucleic Acids Res.* **2000**, *28*, 2413−2419.

(9) Magoshi, J.; Magoshi, Y.; Becker, M. A.; Nakamura, S. Biospinning (Silk fiber formation, multiple spinning mechanisms). In *Polymeric Materials Encyclopedia*; Salomore, J. C., Ed.; CRC Press: Boca Racton, FL, 1996; 119, p 669.

(10) Foo, C. W. P.; Bini, E.; Hensman, J.; Knight, D. P.; Lewis, R.; Kaplan, D. L. *Applied Physics A*: *Materials Science and Processing*; in press; published online Nov 19, 2005.

(11) Altman, G. H.; Diaz, F.; Jakuba, C.; Calabro, T.; Horan, R. L.; Chen, J.; Lu, H.; Richmond, J.; Kaplan, D. L. *Biomaterials* **2003**, *24*, 401−416.

(12) Minora, N.; Tsukada, M.; Nagura, M. *Biomaterials* **1990**, *11*, 430−434.

(13) Panilaitis, B.; Altman, G. H.; Chen, J.; Jin, H. J.; Karageorgiou, V.; Kaplan, D. L. *Biomaterials* **2003**, *24*, 3079−3085.

(14) Meinel, L.; Hofmann, S.; Karageorgiou, V.; Kirker-Head, C.; McCool, J.; Gronwicz, G.; Zichner, L.; Langer, R.; Vunjak-Novakovic, G.; Kaplan, D. L. *Biomaterials* **2004**, *26*, 147−155.

(15) Horan, R.; Antle, K.; Collette, A.; Wang, Y.; Huang, J.; Moreau, J.; Volloch, V.; Kaplan, D. L.; Altman, G. H. *Biomaterials* **2005**, *26*, 3385−3393.

(16) Nazarov, R.; Jin, H. J.; Kaplan, D. L. *Biomacromolecules* **2004**, *5*, 718−726.

(17) Kim, U. J.; Park, J.; Kim, H. J.; Wada, M.; Kaplan, D. L. *Biomaterials* **2005**, *26*, 2775−2785.

(18) Jin, H. J.; Park, J.; Kim, U. J.; Valluzzi, R.; Cebe, P.; Kaplan, D. L. *Biomacromolecules* **2004**, *5*, 711−717.

(19) Jin, H. J.; Park, J.; Karageorgiou, V.; Kim, U. J.; Valluzzi, R.; Cebe, P.; Kaplan, D. L. *Adv. Funct. Mater.* In press.

(20) Sofia, S.; McCarthy, M. B.; Gronowicz, G.; Kaplan, D. L. *J. Biomed. Mater. Res.* **2001**, *54*, 139−148.

(21) Jin, H. J.; Fridrikh, S. V.; Rutledge, G. C.; Kaplan, D. L. *Macromolecules* **2002**, *3*, 1233−1239.

(22) Wang, M.; Jin, H. J.; Kaplan, D. L.; Rutledge, G. C. *Macromolecules* **2004**, *37*, 6856−6864.

(23) Altman, G.; Stark, P.; Horan, R.; Lu, H.; Vunjak-Novokovic, G.; Kaplan, D. L. *Biomech. Eng.* **2002**, *124*, 742−749.

(24) Altman, G.; Horan, R.; Lu, H.; Moreau, J.; Martin, I.; Richmond, J. C.; Kaplan, D. L. *Biomaterials* **2002**, *23*, 4131−4141.

(25) Kim, U. J.; Park, J.; Li, C.; Jin, H. J.; Valluzzi, R.; Kaplan, D. L. *Biomacromolecules* **2004**, *5*, 786−792.

(26) Kamath, K. R.; Park, K. *Adv. Drug. Delivery Rev.* **1993**, *11*, 59−84and references therein.

(27) Jin, H.-J.; Kaplan, D. L. *Nature* **2003**, *424*, 1057−1061.

(28) Zhou, Li, Chen, X.; Shao, Z.; Huang, Y.; Knight, D. P. *J. Phys. Chem. B* **2005**, *109*, 16937−16945.

(29) Byler, D. M.; Susi, H. *Biopolymers* **1986**, *25*, 469−487.

(30) Arrondo, J. L. R.; Muga, A.; Castresena, J.; Goni, F. M. *Prog. Biophys. Mol. Biol.* **1993**, *59*, 23−56.

(31) Dong, A.; Huang, P.; Caughey, W. *Biochemistry* **1990**, *29*, 3303−3308.

(32) Speare, J. O.; Rush, T. S. *Biopolymers* **1990**, *72*, 193−204.

(33) Wilson, D.; Valluzzi, R.; Kaplan, D. L. *Biophys. J.* **2000**, *78*, 2690−2701.

(34) Tretinnikov, O. N.; Tamada, Y. *Langmuir* **2001**, *17*, 7406−7413.

(35) Decko, C.; Knight, D.; Kenny, J.; Vollrath, F. *Biomacromolecules* **2004**, *5*, 758−767.

(36) Kenny, J. M.; Knight, D.; Wise, M. J.; Vollrath, F. *Eur. J. Biochem.* **2002**, *269*, 4159−4163.

(37) Decko, C.; Kenny, J. M.; Knight, D.; Vollrath, F. *Biochemistry* **2004**, *43*, 14080−14087.

(38) Valluzzi, R.; Szela, S.; Avtges, P.; Kirschner, D.; Kaplan, D. *J. Phys. Chem. B* **1999**, *103*, 11382−11392.

(39) Asakura, T.; Kuzuhara, A.; Tabeta, R.; Saito. H. *Macromolecules* **1985**, *18*, 1841−1845.

(40) Chen, X.; Knight, D. P.; Shao, Z.; Vollrath, F. *Polymer* **2001**, *42*, 9969−9974.

(41) Ayub, Z. H.; Arai, M.; Hirabayashi, K. *Biosci., Biotechnol., Biochem.* **1993**, *57*, 1910−1912.

(42) Hanawa, T.; Watanabe, A.; Tsuchiya, T.; Ikoma, R.; Hidaka, M.; Sugihara, M. *Chem. Pharm. Bull.* **1995**, *43*, 284−288.

(43) Kang, G. D.; Nahm, J. H.; Park, J. S.; Moon, J. Y.; Cho, C. S.; Yeo, J. H. *Marcromol. Rapid Commun.* **2000**, *21*, 788−791.

(44) Urry, D. W.; Peng, S. Q.; Xu, J.; McPherson, D. T. *J. Am. Chem. Soc.* **1997**, *19*, 11161−11162.

(45) Luan, C. H.; Harris, R. D.; Prasad, K. U.; Urry, D. W. *Biopolymers* **1990**, *29*, 1699−1706.

(46) Nagersekar, A.; Crissman, J.; Crissman, M.; Ferrari, F.; Cappello, J. *J. Biomed. Mater. Res.* **2002**, *62*, 195−203.

(47) Edsall, J. T.; McKenzie, H. A. *Adv. Biophys.* **1983**, *16*, 53−183.

(48) Urry, D. W. *Angew. Chem., Int. Ed. Engl.* **1993**, *32*, 819−841.

(49) Terry, A. E.; Knight, D. P.; Porter, D.; Vollath, F. *Biomacromolecules* **2004**, *5*, 768−772.

(50) Zhou, P.; Xie, X.; Knight, D. P.; Zong, X.-H.; Deng, F.; Yao, W.-H. *Biochemistry* **2004**, *43*, 11302−11311.

(51) Zhou, L.; Chen, X.; Shao, Z.; Huang, Y.; Knight, D. P. *J. Phys. Chem. B* **2005**, *109*, 16937−16945.

(52) Feil, H.; Bae, Y. H.; Feijen, J.; Kim. S. W. *Macromolecules* **1993**, *26*, 2496−2500.

(53) Yamamoto, K.; Serizawa, T.; Muraoka, Y.; Akashi, M. *Macromolecules* **2001**, *34*, 8014−8020.

(54) Jones, M. S. *Eur. Polym. J.* **1999**, *35*, 795−801.

(55) Smith, D. A.; Wallwork, M. L.; Zhang, J.; Kirkham, J.; Robinson, C.; Marsh, A.; Wong, M. *J. Phys. Chem. B* **2000**, *104*, 8862−8870.

(56) Mautner, M. M.-N.; Elmore, D. E.; Scheiner, S. *J. Am. Chem. Soc.* **1999**, *121*, 7625−7635.

(57) Kawasaki, H.; Sasaki, S.; Maeda, H. *J. Phys. Chem. B* **1997**, *101*, 5089−5093.

(58) Urry, D. W. *J. Phys. Chem. B* **1997**, *101*, 11007−11028.

(59) Koga, S.; Sasaki, S.; Maeda, H. *J. Phys. Chem. B* **2001**, *105*, 4105−4110.

(60) Kawashima, T.; Koga, S.; Annaka, M.; Sasaki, S. *J. Phys. Chem. B* **2005**, *109*, 1055−1062.

(61) Urry, D. W. *Angew. Chem., Int. Ed. Engl.* **1993**, 32, 819−841. Urry, D. W. *Angew. Chem., Int. Ed. Engl.* **1993**, 32, 16937−16945.